Supporting Information for:

Enhanced Annihilation Electrochemiluminescence by Nano-fluidic Confinement

Hanan Al-Kutubi,[§] Silvia Voci,[#] Liza Rassaei,[‡,¶] Neso Sojic,[,#] and Klaus Mathwig*[,§]*

§ University of Groningen, Groningen Research Institute of Pharmacy, Pharmaceutical Analysis, P.O. Box 196, 9700 AD Groningen, The Netherlands

Univ. Bordeaux, CNRS UMR 5255, Bordeaux INP, Site ENSCBP, 33607 Pessac, France

‡ Rotterdam School of Management, Erasmus University, Burgemeester Oudlaan 50, 3062 PA Rotterdam, The Netherlands

¶ Delft University of Technology, Van der Maasweg 9, 2629 HZ Delft, The Netherlands

Email: neso.sojic@enscbp.fr; k.h.mathwig@rug.nl

Contents

1. Chemical reagents

Tris(2,2'-bipyridine)ruthenium(II) hexafluorophosphate ($Ru(bpy)_3(PF_6)_2$), sulfuric acid and the supporting electrolyte tetrabutylammonium hexafluorophosphate ($TBAPF_6$) were purchased from Sigma-Aldrich, chromium etchant (Selectipur) from BASF. All solutions were prepared using Milli-Q water (resistivity = 18 MΩ cm) or HPLC-grade acetonitrile (Sigma-Aldrich).

2. Device Fabrication

Figure S1 shows the fabrication steps of electrochemical nanofluidic devices. See ref. 1 for further details of the process. Process parameters were optimized to accommodate the properties of a transparent borosilicate substrate in contrast to substrates of opaque oxidized Si wafers used previously.

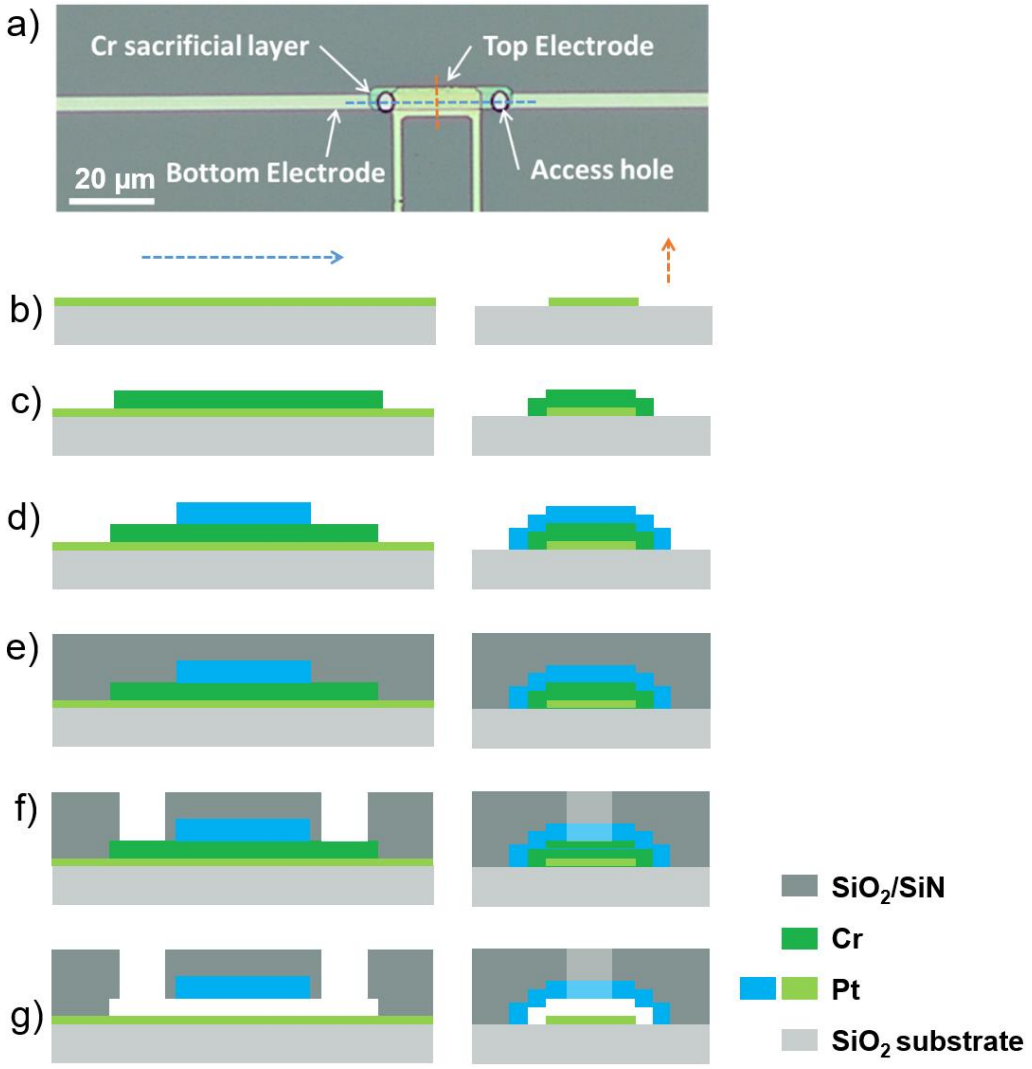

Figure S1: *Microfabrication steps of transparent nanofluidic electrochemical transducers. a) Top-view micrograph of a device, indicating the longitudinal (blue dashed line) and lateral (orange) cross section in the schematic below. b) Patterning of a 20-nm-thick Pt layer by photolithography, metal evaporation and a lift-off process. A 10-cm-wide and 700-µm-thick borosilicate wafer substrate was used. c) Photolithography, metal evaporation, and lift-off to structure the Cr layer defining the nanochannel volume. d) Photolithography, Pt evaporation and lift-off to define the top electrode. e) PECVD deposition of a SiO_2/SiN/SiO_2 passivation layer. f) photolithography and reactive ion etching of access holes through the passivation layer using the resist as mask. g) The wafer is diced into individual chips. Directly before and experiment, the Cr layer is removed and the nanochannel is formed using a selective wet chemical Cr etch.*

3. Background measurement with one electrode

As a control, an experiment was performed where the bottom electrode of a nanofluidic device was disconnected (i.e., kept at a floating potential) while the top electrode was pulsed between 0 V and 2.0 V vs. Ag wire. The chronoamperometric current and light intensity response measured with a photomultiplier tube are both shown in Figure S2.

While pulsing a single electrode, the change in detected light intensity is negligible compare to the background intensity. This observation demonstrates that two independently biased electrodes (at constant) potentials are necessary for the generation of electrochemiluminescence; indicating that light generation takes place according to the annihilation pathway shown in reactions (1-4) in the main text.

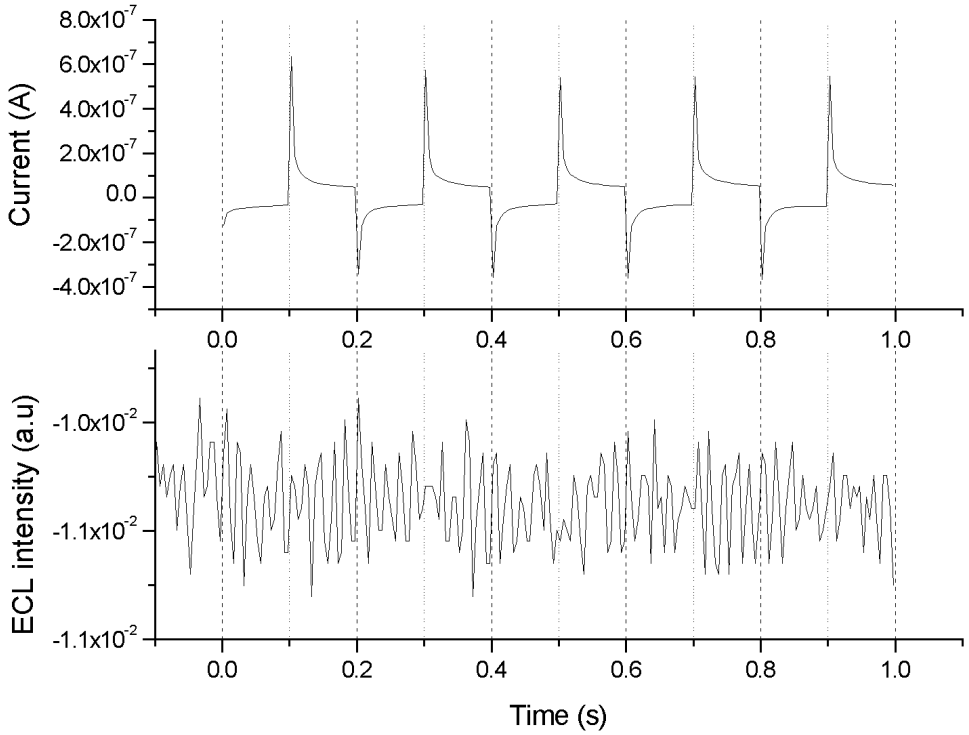

***Figure S2**: Measured chronoamperometric currents (top) and corresponding light intensity recorded with a PMT (bottom). A potential alternating between 0 V and 2.0 V vs. Ag was applied to the top electrode of a nanogap device while the bottom electrode was kept floating. A solution of 10 mM $Ru(bpy)_3(PF_6)_2$ and 0.1 M $TBAPF_6$ in acetonitrile was used.*

4. Finite element modeling

Two-dimensional finite element modeling **(**COMSOL Multiphysics 5.2a) was employed to determine steady-state concentration profiles of the different $Ru(bpy)_3$ ion species. The geometry consists of the channel itself with a length of overall 20 µm and a height of 100 nm. 2 µm wide access holes at both ends of the channel couple the nanochannel to a larger reservoir. The top electrode is defined as a 20-µm-long segment in the center of the upper boundary of the nanochannel, while the bottom electrode covers the entire channel floor segment.

For the simulation, we considered diffusion as the only mass transport mechanism (i.e., no convection, and no electrical migration at a high concentration of background electrolyte) described by Fick's second law:[2]

$$\frac{\partial c_j}{\partial t} = D\nabla^2 c_j$$

Here, $c_{j=1,2,3,4}$ denotes the concentrations of the four compounds $[Ru(bpy)_3]^+$, $[Ru(bpy)_3]^{2+}$, $[Ru(bpy)_3]^{3+}$, and $[Ru(bpy)_3]^{2+}$*, respectively. We assumed an equal diffusion coefficient of $D = 1\times10^{-9}$ m^{2}s^{-1} for all species.[3] A starting concentration of 10 mM $[Ru(bpy)_3]^{2+}$ was chosen in the entire simulation geometry, and a reservoir boundary was set to a constant concentration of also 10 mM $[Ru(bpy)_3]^{2+}$ (boundary and starting conditions of 0 M $[Ru(bpy)_3]^+$, 0 M $[Ru(bpy)_3]^{3+}$, and 0 mM $[Ru(bpy)_3]^{2+}$*).

To determine concentration profiles in annihilation mode we simulated four reactions as shown in the main text:

$$[Ru(bpy)_3]^{2+} + e^- \rightarrow [Ru(bpy)_3]^+ \quad (1)$$

$$[Ru(bpy)_3]^{2+} - e^- \rightarrow [Ru(bpy)_3]^{3+} \quad (2)$$

$$[Ru(bpy)_3]^+ + [Ru(bpy)_3]^{3+} \xrightarrow{k_{ann}} [Ru(bpy)_3]^{2+} + [Ru(bpy)_3]^{2+*} \quad (3)$$

$$[Ru(bpy)_3]^{2+*} \xrightarrow{k_4} [Ru(bpy)_3]^{2+} + h\nu \quad (4)$$

In addition, we considered the possibility of 2-electron reactions at the electrodes (which occur when $[Ru(bpy)_3]^+$ or $[Ru(bpy)_3]^{3+}$ crosses the nanochannel without participating in annihilation):

$$[Ru(bpy)_3]^{3+} + 2e^- \rightarrow [Ru(bpy)_3]^+ \quad (5)$$

$$[Ru(bpy)_3]^+ - 2e^- \rightarrow [Ru(bpy)_3]^{3+}. \quad (6)$$

At the electrode surfaces, we implemented a Butler-Volmer formalism[4] calculating normal molar influxes N_j at the positively biased top electrode (species 1, 2 and 4 are consumed, and an influx N_3 of species 3 is generated):

$$N_1 = k_{13,f}c_3 - k_{13,b}c_1 \quad (7)$$

$$N_2 = k_{23,f}c_3 - k_{23,b}c_2 \quad (8)$$

$$N_3 = k_{23,b}c_2 - k_{23,f}c_3 + k_{23,b}c_4 + k_{13,b}c_1 - k_{13,f}c_3 \quad (9)$$

$$N_4 = -k_{23,b}c_4, \quad (10)$$

and at the bottom electrode (negative bias, normal influx N_1 of $[Ru(bpy)_3]^+$, consumption of all other ions):

$$N_1 = k_{21,b}c_2 - k_{21,f}c_1 + k_{21,b}c_4 + k_{31,b}c_3 - k_{31,f}c_1 \quad (11)$$

$$N_2 = k_{21,f}c_1 - k_{21,b}c_2 \quad (12)$$

$$N_3 = k_{31,f}c_1 - k_{31,b}c_3 \quad (13)$$

$$N_4 = -k_{21,b}c_4. \quad (14)$$

Here, the forward and backward rate constants are defined as:

$$k_{13,f} = k_{23,f} = k_0 \exp\left[\frac{-\alpha F(E_{\text{top}} - E_{h(\text{ox})})}{RT}\right] \quad (15)$$

$$k_{13,b} = k_{23,b} = k_0 \exp\left[\frac{(1-\alpha) F(E_{\text{top}} - E_{h(\text{ox})})}{RT}\right] \quad (16)$$

$$k_{31,f} = k_{32,f} = k_0 \exp\left[\frac{-\alpha F(E_{\text{bot}} - E_{h(\text{red})})}{RT}\right] \quad (17)$$

$$k_{31,b} = k_{32,b} = k_0 \exp\left[\frac{(1-\alpha) F(E_{\text{bot}} - E_{h(\text{red})})}{RT}\right]. \quad (18)$$

F, *R*, and *T* are the Faraday constant, gas constant and temperature, respectively, $\alpha = 0.5$ the charge transfer coefficient. A high standard rate constant of $k_0 = 0.01$ m s^{-1} was chosen for all electrode reactions. For the difference of the applied potentials (at the top and bottom electrode, respectively) and the formal respective potentials for oxidation/reduction we chose the same high overpotentials as in the experiment ($E_{\text{top}} = 2$ V, $E_{\text{red}} = -1.5$ V, $E_{h(\text{ox})} = 1.35$ V, $E_{h(\text{red})} = -1.27$ V).

In the bulk of the nanochannel, we implemented eq. (3,4) as reactions R_j (in M s^{-1}) of the generation and consumption of species with concentrations c_j:

$$R_1 = -k_{\text{ann}} c_1 c_3 \quad (19)$$

$$R_2 = k_{\text{ann}} c_1 c_3 + k_4 c_4 \quad (20)$$

$$R_3 = -k_{\text{ann}} c_1 c_3 \quad (21)$$

$$R_4 = k_{\text{ann}} c_1 c_3 - k_4 c_4. \quad (22)$$

For the concentration profiles shown in Figure 5c,d in the main text we considered a fast annihilation rate of $k_{\text{ann}} = 10^{10}$ M^{-1} s^{-1} as well as a lifetime of the excited state $[Ru(bpy)_3]^{3+}$* of 1 µs ($k_4 = 10^6$ s^{-1}). Light generation hν was not considered explicitly.

Due to the fast efficient annihilation with the rate k_{ann} the vast majority of generated species $[Ru(bpy)_3]^{+}$ and $[Ru(bpy)_3]^{3+}$ undergo annihilation in the bulk nanochannel, reducing their concentrations to almost 0 mM at the top and bottom electrode, respectively. Therefore, the current obtained is almost exclusively due to the 1-electron processes (1,2) taking place, dominating 2-electron processes (5,6).

The sum of the concentration of $[Ru(bpy)_3]^{2+}$ and $[Ru(bpy)_3]^{2+}$* in the center of the channel (z=50 nm) amounts to approximately 8 mM. An infinitely fast annihilation would lead to a concentration of 10 mM.

The concentration of $[Ru(bpy)_3]^{2+}$* and hence the ratio of concentrations of $[Ru(bpy)_3]^{2+}$* to $[Ru(bpy)_3]^{2+}$ is determined by k_4 (4), i.e., by the lifetime of the excited state. For the chosen k_4-value, a ratio of about 1:3 was obtained. The $[Ru(bpy)_3]^{2+}$* concentration profile shows that light is emitted predominantly from the vertical symmetry plane of the nanochannel.

To simulate concentration profiles in redox cycling mode (Fig. 5a,b in the main text), we considered oxidation at the top electrode:

$$N_2 = k_{23,f} c_3 - k_{23,b} c_2 \quad (22)$$

$$N_3 = k_{23,b} c_2 - k_{23,f} c_3, \quad (23)$$

and reduction at the bottom electrode:

$$N_2 = k_{23,f} c_3 - k_{23,b} c_2 \quad (24)$$

$$N_3 = k_{32,f} c_2 - k_{32,b} c_3. \quad (25)$$

At the chosen high overpotentials, linear concentration profiles are established across the nanochannel as expected.[5] (Only the standard potential $E_{h(\mathrm{ox})}$ and a potential of the bottom electrode of $E_{\mathrm{red}} = 0$ V were used for simulating the redox cycling mode).

5. Numerical concentration profiles

5.1 Variation of exited-state lifetime

To explore the effect of the lifetime of the excited $[Ru(bpy)_3]^{2+*}$ luminophore state on concentration profiles in the nanochannel, we varied it in a two-dimensional COMSOL simulation from 10 µs ($k_4 = 10^5$ s^{-1}) to 1 µs ($k_4 = 10^6$ s^{-1} as shown in Fig. 5 in the main text) to 0.1 µs ($k_4 = 10^7$ s^{-1}). Simulated concentration profiles in annihilation mode are shown in Figure S3.

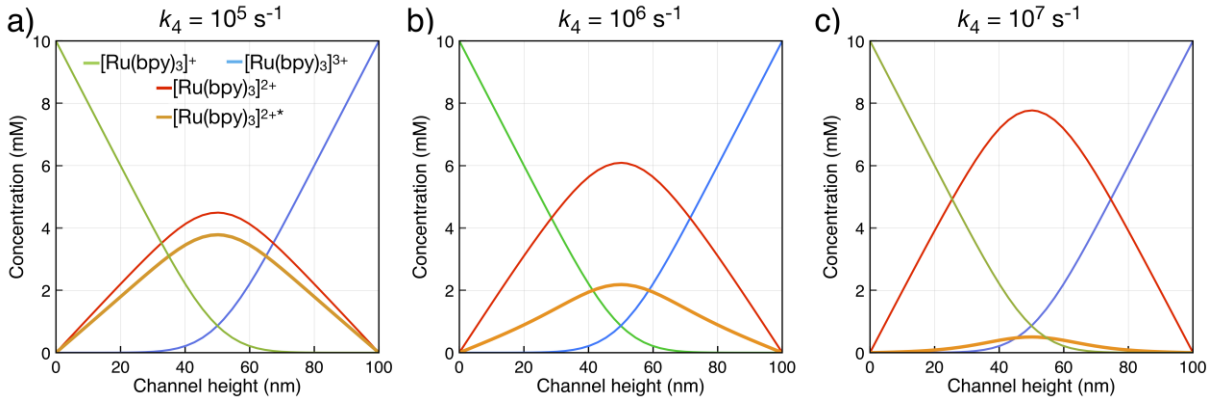

Figure S3: *Finite element simulation of concentration profiles of a 10 mM $[Ru(bpy)_3]^{2+}$ bulk concentration in the nanochannel. Cross-sectional profiles of a two-dimensional numerical geometry are shown. The lifetime of the excited state is a) 10 µs, b) 1 µs, and c) 0.1 µs.*

For a lifetime longer than the diffusion time across (half) the channel (see Fig. S3a), a large flux of excited-state ions to the electrodes is observed (evident by the steep slope of the orange graph at z = 0 nm and z = 100 nm in Fig. S3a). In this case, a majority of $[Ru(bpy)_3]^{2+*}$ ions reacts at the electrodes before emitting a photon.

For very short-lived excited luminophore states (see Fig. S3c), their flux towards the electrode is reduced to virtually 0, and all of them relax to the ground state.

In the likely experimental case of a $[Ru(bpy)_3]^{2+*}$ lifetime of 1 µs (see Fig. S3b and Fig. 5 in the main text), most luminophores will relax to the ground state before reaching an electrode by diffusion (the concentration of $[Ru(bpy)_3]^{2+*}$ is less than half of the $[Ru(bpy)_3]^{2+}$ concentration at any position across the nanochannel). Nonetheless, a considerable amount of $[Ru(bpy)_3]^{2+*}$ is oxidized or reduced before the end of their lifetime and will not contribute to ECL emission.

5.2 Variation of nanochannel height

We changed the height of the nanochannel in the numerical simulation to elucidate its effect on concentration profiles and expected ECL intensity as shown in Figure S4 for channel heights of 50 nm, 100 nm, 200 nm, and 500 nm.

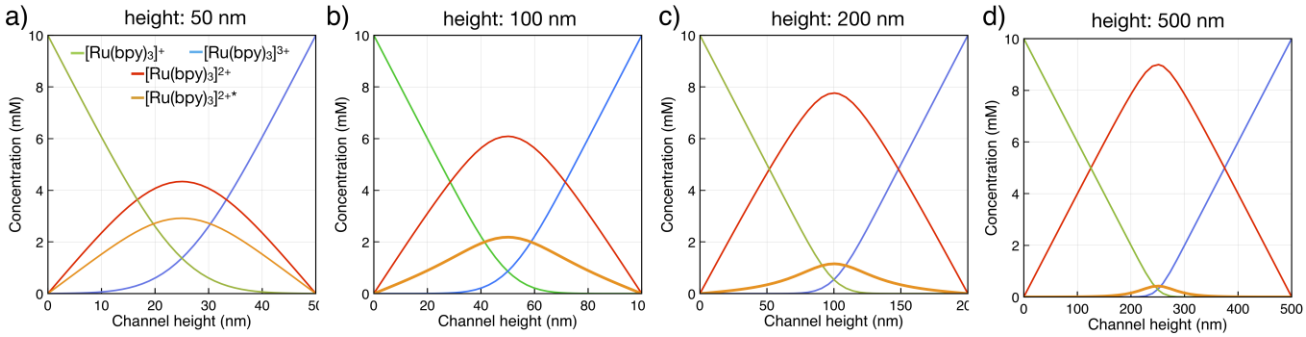

Figure S4: *Finite element simulation of concentration profiles of a 10 mM $[Ru(bpy)_3]^{2+}$ bulk concentration for various channel heights of a) 50 nm, b) 100 nm, c) 200 nm, and d) 500 nm. The lifetime of the $[Ru(bpy)_3]^{2+*}$ state was set at 1 µs ($k_4 = 10^6\ s^{-1}$). (Panel (b) is identical to Fig. 5d in the main text.)*

The effect of a changed height (and, thus, different diffusion times across the channel) on the profiles is comparable to the effect of varied lifetimes: For diffusion times longer than excited-state lifetimes, a greater number of luminophores emit light before reaching an electrode surface (e.g., at heights of 200 nm and 500 nm).

With an increased channel height, the diffusion time also increases as compared to the high annihilation rate of $k_{ann} = 10^{10}\ M^{-1}\ s^{-1}$. Therefore, $[Ru(bpy)_3]^{2+}$ profiles shift from a "parabolic" to a sharp "triangular" shape.

We predict that changing the nanochannel height will have various effects on the intensity of light emission: Overall, emission will increase *linearly* with decreased height. (Intensity would increase *quadratically* as diffusion times are reduced quadratically. However, the channel volume, and, thus, the number of molecules participating in ECL, is also reduced linearly for shallower channels). In addition, if the channel is very shallow, light emission will decrease as oxidation/reduction starts to dominate relaxation and photon emission. We estimate that our experimental nanochannel height of 100 nm could correspond to a value close to the maximum of light emission for a $[Ru(bpy)_3]^{2+*}$ lifetime of 1 µs.

5.3 Degradation of $[Ru(bpy)_3]^+$

We numerically evaluate a possible effect of degradation of $[Ru(bpy)_3]^{3+}$ or $[Ru(bpy)_3]^+$ ions by contaminants on profiles of concentration and light emission. An exemplary degradation reaction is

$$[Ru(bpy)_3]^+ + O_2^- \xrightarrow{k_{deg}} P_1. \qquad (26)$$

Oxidized $[Ru(bpy)_3]^+$ ions react to a product P_1, which does not participate in ECL annihilation anymore. To simulate such a reaction, we added a degradation term to equation (19), it is replaced by

$$R_1 = -k_{ann} c_1 c_3 - k_{deg} c_1. \qquad (27)$$

This means, the concentration c_1 of $[Ru(bpy)_3]^+$ is continously reduced in the bulk of the nanochannel (and reservoir) at a rate k_{deg}. The expected effect on concentration profiles *along* the nanochannel is shown in Figure S5.

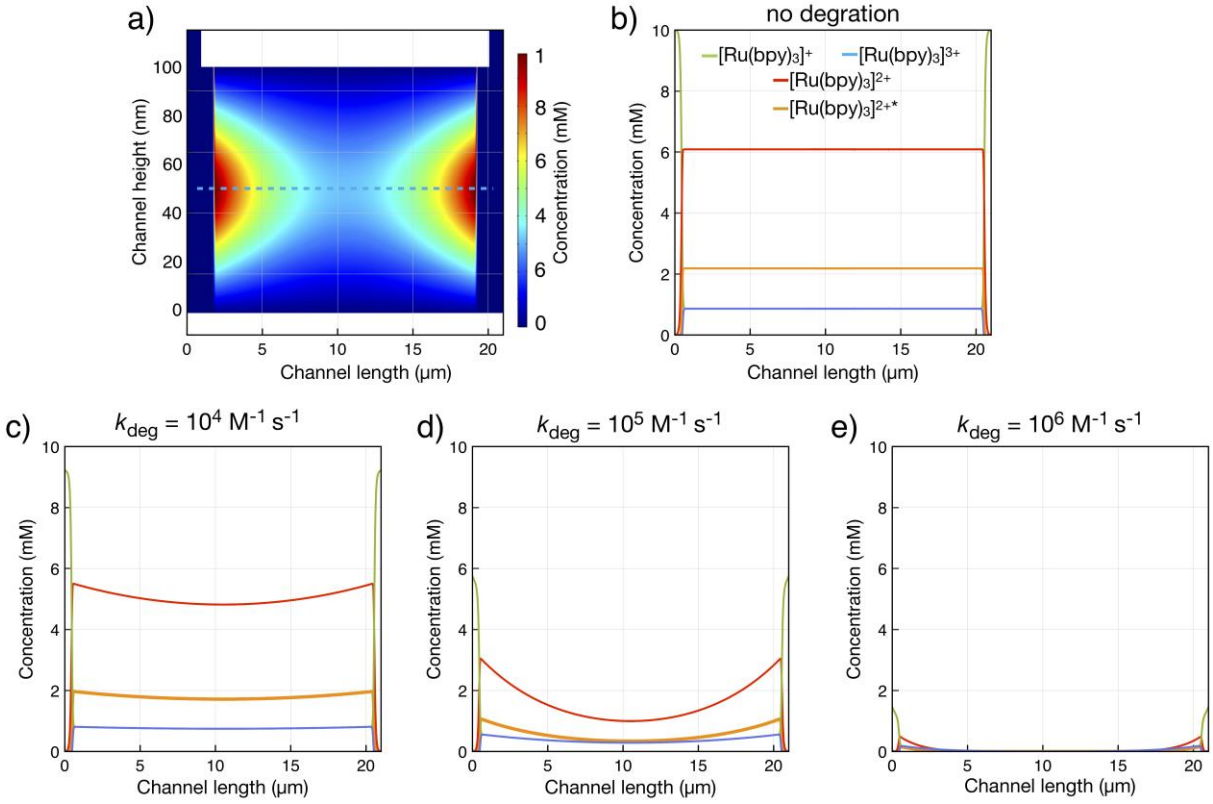

Figure S5: *Finite element simulation of concentration profiles of a 10 mM $[Ru(bpy)_3]^{2+}$ bulk concentration for varied rates of $[Ru(bpy)_3]^+$ degradation k_{deg} (and $k_4 = 10^6\ s^{-1}$; $k_{ann} = 10^{10}\ M^{-1}\ s^{-1}$). a) Two-dimensional $[Ru(bpy)_3]^{+*}$ profile for $k_{deg} = 10^5\ M^{-1}\ s^{-1}$. (b-e) Corresponding profiles* along *the channel (dashed line in a) for: b) no degradation c) $k_{deg} = 10^4\ M^{-1}\ s^{-1}$, c) $k_{deg} = 10^5\ M^{-1}\ s^{-1}$ a (orang curve corresponds to two-dimensional profile in a) and, e) $k_{deg} = 10^6\ M^{-1}\ s^{-1}$.*

The concentration of $[Ru(bpy)_3]^{+*}$ *along* the channel center is proportional to the intensity of emitted light. By comparison to the experimentally determined light emission profile (see Figure 3b in the main text), which shows homogenous intensity along the channel, we estimate that potential degradation by contaminants is limited to a rate lower than about 10^4 M^{-1} s^{-1}.

References

1 S. Kang, K. Mathwig and S. G. Lemay, *Lab Chip*, 2012, **12**, 1262–7.

2 H. R. Zafarani, K. Mathwig, E. J. R. Sudhölter and L. Rassaei, *J. Electroanal. Chem.*, 2016, **760**, 42–47.

3 C. Amatore, B. Fosset, K. M. Mannes and M. R. Wightman, *Anal. Chem.*, 1993, **65**, 2311–2316.

4 G. Valenti, S. Scarabino, B. Goudeau, A. Lesch, M. Jović, E. Villani, M. Sentic, S. Rapino, S. Arbault, F. Paolucci and N. Sojic, *J. Am. Chem. Soc.*, 2017, **139**, 16830–16837.

5 K. Mathwig and S. G. Lemay, *Electrochim. Acta*, 2013, **112**, 943–949.